

Provenance-Driven Reliable Semantic Medical Image Vector Reconstruction via Lightweight Blockchain-Verified Latent Fingerprints

Mohsin Rasheed
 Augusta University
 mrasheed@augusta.edu

Abdullah Al-Mamun
 Augusta University
 aalmamun@augusta.edu

Abstract

Medical imaging is essential for clinical diagnosis, yet real-world data frequently suffers from corruption, noise, and potential tampering, challenging the reliability of AI-assisted interpretation. Conventional reconstruction techniques prioritize pixel-level recovery and may produce visually plausible outputs while compromising anatomical fidelity, an issue that can directly impact clinical outcomes. We propose a semantic-aware medical image reconstruction framework that integrates high-level latent embeddings with a hybrid U-Net architecture to preserve clinically relevant structures during restoration. To ensure trust and accountability, we incorporate a lightweight blockchain-based provenance layer using scale-free graph design, enabling verifiable recording of each reconstruction event without imposing significant overhead. Extensive evaluation across multiple datasets and corruption types demonstrates improved structural consistency, restoration accuracy, and provenance integrity compared with existing approaches. By uniting semantic-guided reconstruction with secure traceability, our solution advances dependable AI for medical imaging, enhancing both diagnostic confidence and regulatory compliance in healthcare environments.

1. Introduction

1.1. Motivation

Medical imaging plays a central role in modern diagnostics, with modalities such as MRI, CT, and X-ray enabling detailed visualization of internal anatomy [29]. The quality and integrity of these images directly affect clinical decisions, yet real-world imaging data are frequently degraded by noise [26], acquisition and compression artifacts [13], or even intentional tampering [4, 43, 50] and device-level attacks [56], all of which can undermine diagnostic reliability. Standard reconstruction methods [4, 13, 31, 43, 50] focus primarily on pixel-level recovery, which can restore visually plausible content but fail to preserve critical anatom-

ical structures. This gap presents a significant challenge for dependable AI systems that aim to assist or automate diagnosis.

Recent advances in deep generative models, including U-Net [17, 34], GANs [20, 60], and diffusion-based architectures [21], have improved inpainting and image restoration tasks. However, these methods remain largely agnostic to the underlying semantic content of medical images. In clinical scenarios, even small structural deviations can lead to incorrect interpretations [29], making semantic fidelity as important as visual similarity. For example, a GAN-based attack [39] changed a lung-cancer scan in seconds and escaped expert detection and a one-pixel perturbation [49] flipped diagnostic output. Furthermore, existing approaches [6, 24, 42, 58] lack mechanisms to verify or track the provenance of reconstructed images, which is crucial for auditing, reproducibility, and clinical trust.

1.2. Proposed Approach and Challenges

To address these limitations, we propose a semantic-aware reconstruction framework that operates directly on *vector embeddings of medical images*, rather than solely on pixels, and leverages high-level latent fingerprints to guide restoration of corrupted data. By conditioning the model on these embeddings extracted from verified image data, our approach ensures that reconstructed structures remain consistent with clinically relevant patterns. In addition, we integrate a lightweight blockchain-based provenance layer, which anchors each reconstruction event in a verifiable ledger. Such integration establishes tamper-evident traceability, decentralized trust, and verifiable data lineage across reconstruction pipelines, essential properties [28] for clinical imaging where authenticity and accountability are paramount. This combination allows not only accurate reconstruction but also traceable, auditable verification of every image modification, ensuring both reliability and trustworthiness.

Despite blockchain's promise for ensuring trust and reliability, its direct adoption in medical imaging introduces several practical challenges. First, conventional blockchain con-

sensus mechanisms [3, 33, 59] such as PoW or BFT incur significant computational and latency overhead, incompatible with real-time or high-throughput image reconstruction tasks. Second, maintaining a complete ledger of reconstruction operations can impose excessive storage and bandwidth costs, especially when handling large-scale image datasets [52]. Third, the high latency of block confirmation [35, 41] undermines the responsiveness needed for time-sensitive diagnostic scenarios. Finally, existing blockchain frameworks often assume persistent peer connectivity, whereas medical imaging workflows may span intermittently connected hospital systems or cloud-edge environments [1, 5].

1.3. Our Contributions

To address these challenges, we design and implement provenance-secured semantic image reconstruction for medical applications (PROSIMA), a system that integrates a U-Net-based reconstruction backbone augmented with semantic consistency guidance from pre-trained embeddings (e.g., Contrastive Language–Image Pretraining-CLIP or medical feature extractors). By conditioning reconstruction on latent fingerprints anchored in a lightweight, scale-free blockchain, PROSIMA ensures tamper-evident verification, traceability, and clinically faithful reconstruction. The system introduces innovations in consensus efficiency, adaptive sharding, distributed load balancing, and storage optimization tailored for vector data. Our framework is designed for robustness and generalization across multiple datasets and corruption types. By explicitly incorporating semantic guidance, perceptual quality metrics, and blockchain-anchored fingerprints, the proposed method bridges the gap between conventional pixel-focused reconstruction and the stringent requirements of dependable AI in medical imaging. Experiments demonstrate superior performance in structural fidelity, semantic consistency, and provenance verification compared to state-of-the-art baselines.

In summary, the paper makes the following core technical contributions:

(i) Semantic-aware Reconstruction Framework: A semantic-aware, provenance-verified image reconstruction pipeline based on a hybrid U-Net backbone, augmented with high-level embeddings and latent fingerprints anchored on a lightweight blockchain, ensuring clinically faithful and tamper-evident reconstructions.

(ii) Geographically Fragmented Ledger Consensus: A set of lightweight blockchain protocols leveraging the *Geographic Fragmentation Technique* (GFT) and the *Scale-Free Graph*-based lightweight consensus mechanism to achieve efficient agreement and cost-effective distributed storage sharding for secure, auditable image management.

(iii) System Prototype: A fully implemented prototype evaluated on a large medical imaging dataset and diverse corruption scenarios, demonstrating superior structural fi-

delity, semantic consistency, and provenance verification compared to mainstream baselines, including: high PSNR (≥ 28.2 dB), strong SSIM (≥ 0.86), robust semantic alignment with embedding cosine similarity (≥ 0.92), a 100% provenance verification rate, and low end-to-end verification latency of approximately 204 ms per image even under severe Gaussian corruption (noise level σ up to 0.10).

2. Related Work

2.1. Deep Learning for Medical Image Reconstruction

Early deep networks for inverse problems treated reconstruction as post-processing of analytic or iterative solutions. FBPCNet demonstrated strong artifact suppression for CT by learning a residual U-Net on top of filtered back-projection [30]. For MR, model-based unrolled methods became dominant: ADMM-Net unfolded an optimization scheme for CS-MRI and learned its proximal operators end-to-end [55]. Variational Networks learned trainable regularizers and data-consistency steps for multi-coil MRI, achieving clinical-quality reconstructions [27]. Learned Primal–Dual further integrated the forward operator within a primal–dual unrolling, improving PSNR/SSIM over TV, U-Net denoisers, and FBP on tomographic tasks [2]. These lines establish that coupling physics with learned priors outperforms pure post-processing. Surveys such as McCann et al. review the design patterns behind these CNN-based inverse solvers [36]. PnP-ADMM replaced proximal steps with powerful denoisers, enabling modular priors with convergence analysis under bounded denoiser assumptions [16, 51]. RED formalized denoiser-defined regularization, further broadening algorithmic choices [44]. These frameworks underpin many practical MRI/CT pipelines by flexibly injecting semantic or learned priors into reconstruction.

2.2. Diffusion/Score-Based Priors for Inverse Problems

Score-based generative models (a.k.a. diffusion models) have recently been used as powerful priors for reconstruction without task-specific supervision. Song et al. trained a score model on medical images and solved CT/MRI inverse problems by posterior sampling guided by physics, showing competitive quality and stronger generalization across measurement models [48]. Subsequent works systematize diffusion for inverse problems and introduce operator-aware or blind formulations (e.g., diffusion posterior sampling, parallel priors for both image and operator) with strong results on MRI and sparse/limited-angle CT [18, 19]. These approaches motivate our semantic conditioning: diffusion priors can be steered by external cues (e.g., embeddings) to improve structure preservation.

Table 1. Comparison of state of the art systems vs PROSIMA.

Category	Semantic	Provenance	Sharding/Scale	Fidelity / Reliability
Vanilla U-Net	No	No	No	Strong low-level fidelity but semantically blind.
CNN/Unrolled Models	Partial	No	No	High fidelity but semantically blind.
Diffusion Models	Indirect	No	No	High realism but obscure traceability.
Semantic Vision-Language Encoders	Yes	No	No	Semantic alignment but no end-to-end reconstruction.
GAN-based Restoration	Limited	No	No	Realistic textures but untraceable.
Classical BFT Blockchains	No	Yes (metadata only)	Partial	No per-image verifiable reconstruction.
PROSIMA (This work)	Yes	Yes	Yes	High semantic fidelity and full traceability.

2.3. Semantic Guidance in Medical Imaging

Semantic encoders provide higher-level anatomical constraints that surpass the limitations of pixel-level losses, enabling reconstruction models to preserve clinically relevant structures. In radiology vision–language (VL) pretraining, BioViL learns joint image–text representations from chest X-rays and corresponding reports, improving semantic alignment and downstream interpretability tasks [10, 12]. Med-CLIP extends this idea by performing contrastive learning on unpaired medical images and reports, achieving strong zero-shot pathology recognition and robust visual–semantic representations for classification and retrieval [53, 54]. *While these models enhance semantic awareness, they lack mechanisms for ensuring structural fidelity, provenance, or tamper-evident reconstruction.*

2.4. Provenance, Trustworthy AI, and Blockchain in Imaging

Trusted medical imaging requires verifiable provenance throughout acquisition, reconstruction, and post-processing stages. Recent efforts toward trustworthy AI emphasize auditability, explainability, and data lineage as essential prerequisites for clinical deployment [28]. In radiology, the ESR white paper highlights blockchain’s potential to ensure integrity and tamper-evidence along imaging data flows, particularly in clinical trials and regulatory pipelines [23].

2.5. Limitations of Current Solutions

Table 1 highlights the shortcomings of current approaches. While deep learning–based reconstruction methods, including U-Net, diffusion priors, and semantic encoders, have achieved remarkable gains in structural preservation, *they fundamentally operate as isolated learning systems with no guarantees on data integrity, reproducibility, or auditability.* U-Net, in particular, remains the most robust and interpretable backbone for medical image reconstruction [7, 22, 30, 45], effectively capturing both global context and fine anatomical detail through its encoder–decoder structure with skip connections, and consistently outperforming transformer- or GAN-based approaches across modalities such as CT [30] and MRI [27]. Compared to diffusion-based priors [47], U-Net models achieve superior performance with

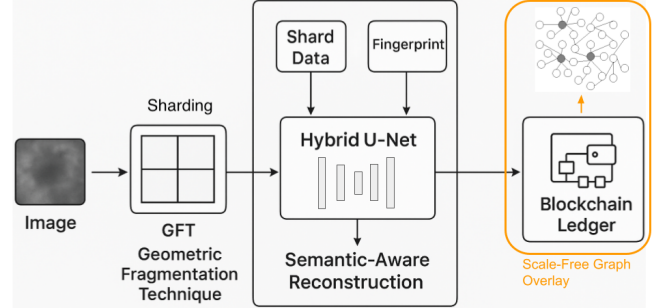


Figure 1. Proposed PROSIMA framework for semantic-aware image reconstruction powered by lightweight blockchain ledger equipped with scale-free graph mechanism and geographic fragmentation technique.

lower computational cost; however, despite these strengths, *no current U-Net-based approach explicitly ensures reliability, reproducibility, or provenance-secured workflows, leaving critical gaps for trustworthy clinical deployment.*

Although blockchain has emerged as a promising direction for securing medical data provenance, there is yet no framework that addresses the unique demands of reliable image reconstruction. Existing blockchain-based imaging systems primarily focus on metadata registration or access control rather than coupling provenance directly with the reconstruction process itself. Notwithstanding these advances, current blockchain frameworks still rely on heavyweight Byzantine Fault Tolerant (BFT) consensus mechanisms [15]. Although designs such as Tendermint [14] and HotStuff [57] improve responsiveness and linearity, they remain unsuitable for high-throughput, computationally intensive imaging workflows for several reasons: **(i)** these protocols introduce significant communication overhead and synchronization latency [35], **(ii)** lack data-local adaptive sharding for large volumetric data, and **(iii)** are unable to guarantee real-time reliability and semantic fidelity during distributed reconstruction. *These limitations collectively motivate the need for a lightweight, domain-optimized blockchain protocol that integrates directly with semantic-aware reconstruction to ensure tamper-evident, provenance-secured, and clinically faithful imaging.*

3. Methodology

3.1. PROSIMA System Overview

PROSIMA performs semantic-aware medical image reconstruction in a distributed environment, targeting three inter-dependent design goals: **(i)** computational reliability, **(ii)** semantic reconstruction quality, and **(iii)** scalability under high-throughput conditions. Figure 1 illustrates the PROSIMA architecture that integrates three tightly coupled components: **(i)** a Geometric Fragmentation Technique (GFT) for deterministic sharding, a **(ii)** Hybrid U-Net for semantic reconstruction, and a **(iii)** scale-free blockchain layer for provenance and reliability.

Each medical image (2D or 3D) is partitioned into K geometrically coherent shards using GFT, which enforces *deterministic fragmentation boundaries*. Unlike random or content-based sharding, GFT guarantees reproducible shard topology across nodes, allowing the system to minimize redundant blockchain replication while ensuring fast shard localization and reaggregation. Deterministic shard IDs eliminate the need for global state synchronization, reducing storage duplication overhead from $O(N)$ to near $O(\log N)$ in the scale-free overlay. These shards are distributed across nodes organized by a scale-free overlay graph [11] with a power-law degree distribution, where high-degree leader nodes maintain both full ledgers and denser shard sets, while low-degree peers store sparse fragments. This configuration inherently supports fault-tolerant redundancy and minimizes synchronization latency.

Reconstruction occurs primarily at an edge node that retrieves only the required shards (locality-first) through a blockchain-guided lookup. Cached semantic embeddings at the edge accelerate reassembly by providing latent priors from previously verified reconstructions. The reconstruction engine employs a *Hybrid U-Net*, which combines convolutional encoders for local texture recovery and transformer-based decoders for global semantic coherence. Conditioning on latent fingerprints retrieved from the blockchain ensures that reconstructed outputs are verifiable and semantically aligned with their original images. Finally, a compact Merkle-root fingerprint of each reconstructed image is anchored on-chain, enabling immutable provenance tracking with minimal blockchain overhead.

The integration of the scale-free blockchain layer addresses the shortcomings of conventional BFT-based systems (e.g., PBFT, Tendermint, HotStuff), which suffer from heavy communication and synchronization costs unsuitable for image-intensive workloads. Instead, PROSIMA employs a lightweight consensus mechanism over the scale-free network, reducing agreement complexity to sub-logarithmic levels and ensuring low-latency validation for provenance updates. This synergy between deterministic geometric fragmentation, hybrid semantic reconstruction, and blockchain-

backed reliability forms the core of PROSIMA’s scalable and trustworthy medical imaging pipeline.

3.2. Problem Definition

Let $I_c \in \mathbb{R}^{H \times W}$ denote a corrupted medical image, and I_o its corresponding original (ground-truth) image. In PROSIMA, each image is first partitioned into K rectangular shards using the GFT:

$$\{I_c^{(k)}\}_{k=1}^K = \text{GFT}(I_c), \quad (1)$$

where each shard $I_c^{(k)}$ is distributed across nodes in a scale-free overlay graph. This fragmentation enables efficient storage, locality-aware retrieval, and parallel reconstruction across distributed nodes.

The goal of semantic-aware reconstruction is to learn a mapping:

$$f_\theta : \{I_c^{(k)}\}_{k=1}^K \mapsto I_r, \quad (2)$$

where I_r is the reconstructed image that preserves both low-level pixel fidelity and high-level semantic structures. Reconstruction is conditioned on a latent fingerprint z^* extracted from verified shards via the blockchain, enabling traceable provenance and reliable reconstruction. Formally, the task is posed as the following optimization problem:

$$\begin{aligned} \min_{\theta} \mathcal{L}_{total}(I_r, I_o) = & \mathcal{L}_{pixel}(I_r, I_o) + \lambda_1 \mathcal{L}_{perceptual}(I_r, I_o) \\ & + \lambda_2 \mathcal{L}_{semantic}(I_r, I_o), \end{aligned} \quad (3)$$

where

- \mathcal{L}_{pixel} is a pixel-wise reconstruction loss (L1 or L2), enforcing low-level fidelity between I_r and I_o , critical for medical details;
- $\mathcal{L}_{perceptual}$ is a perceptual loss computed over high-level features extracted from a pre-trained network (e.g., VGG-16), ensuring structural and textural similarity;
- $\mathcal{L}_{semantic}$ enforces semantic consistency via embeddings from a pre-trained encoder (e.g., Contrastive Language–Image Pretraining-CLIP or medical feature extractor), preserving anatomically meaningful structures.

In PROSIMA, reconstruction uses a *hybrid U-Net generator* G that is conditioned on both:

- $\{I_c^{(k)}\}$ retrieved from distributed nodes (locality-first)
- z^* anchored on the blockchain, encoding semantic priors and verified image characteristics.

The reconstructed image is then obtained as:

$$I_r = G(\{I_c^{(k)}\}_{k=1}^K, z^*), \quad (4)$$

ensuring that I_r is *visually realistic, semantically faithful, and verifiable* via blockchain-based provenance. This formulation explicitly unifies distributed storage, GFT-based sharding, hybrid U-Net reconstruction, and blockchain-verifiable latent fingerprints, providing a rigorous foundation for clinical reliability, semantic accuracy, and system scalability.

Protocol 1 Federated Training of Semantic Reconstruction Models with Ledger Anchoring

```

1: Input: Training dataset  $\mathcal{D}$  across edge nodes, encoder  $E$ , generator  $G$ , semantic extractor  $S$ , hash function  $H$ , blockchain ledger  $L$ 
2: function TRAINANDANCHORMODELS( $\mathcal{D}, E, G, S, H, L$ )
3:   for each local node  $n_i$  in parallel do
4:     for each mini-batch  $(I_o, I_c)$  from  $\mathcal{D}_i$  do
5:        $I_r \leftarrow G(I_o, S(I_c), E(I_o))$             $\triangleright$  Generate reconstruction
6:       Compute losses:
7:        $\mathcal{L}_{total} = \mathcal{L}_{pixel} + \lambda_1 \mathcal{L}_{perceptual} + \lambda_2 \mathcal{L}_{semantic}$ 
8:       Update  $(E, G, S)$  via Adam optimizer
9:     end for
10:     $h_i \leftarrow H(\text{model.weights}_i)$             $\triangleright$  Compute fingerprint
11:     $tx_i \leftarrow \text{CreateTransaction}(h_i, \text{metadata}_i)$             $\triangleright$  Create transaction
12:    ConsensusProtocol( $tx_i$ )            $\triangleright$  Anchor via ledger
13:     $L.\text{commit}(tx_i)$ 
14:  end for
15:   $(E, G, S) \leftarrow \text{Aggregate}(\{(E_i, G_i, S_i)\})$ 
16: Output: Trained models  $E, G, S$  anchored in ledger
17: end function

```

Protocol 2 Latent Fingerprint Anchoring with Deterministic Fragmentation

```

1: Input: Image  $I$ , pretrained encoder  $E$ , hash  $H$ , ledger  $L$ , fragmentation operator  $\mathcal{F}_{GFT}$ 
2: Precondition:  $E$  obtained from Protocol 1
3: function LATENTFINGERPRINT( $I, E, H, L, \mathcal{F}_{GFT}$ )
4:    $\{I_k\}_{k=1}^K \leftarrow \mathcal{F}_{GFT}(I)$ 
5:   for each shard  $I_k$  do
6:      $z_k \leftarrow E(I_k)$ 
7:      $h_k \leftarrow H(z_k)$ 
8:      $tx_k \leftarrow \text{CreateTransaction}(h_k, \text{metadata}_k)$ 
9:     Consensus( $tx_k$ )
10:     $L.\text{commit}(tx_k)$ 
11:  end for
12:   $h_{root} \leftarrow \text{MerkleRoot}(\{h_k\})$ 
13:   $L.\text{commit}(h_{root})$ 
14: Output: Root fingerprint  $h_{root}$ 
15: end function

```

3.3. Training Objective

The reconstruction model is trained to jointly optimize multiple objectives ensuring pixel accuracy, perceptual fidelity, and semantic consistency. Formally, the total loss is defined as:

$$\mathcal{L}_{total} = \mathcal{L}_{pixel} + \lambda_1 \mathcal{L}_{perceptual} + \lambda_2 \mathcal{L}_{semantic}, \quad (5)$$

where \mathcal{L}_{pixel} enforces low-level fidelity (L1 or L2) between the reconstructed image I_r and the original I_o , $\mathcal{L}_{perceptual}$ measures differences in high-level feature representations from a pre-trained network (e.g., VGG) to ensure structural and textural coherence, and $\mathcal{L}_{semantic}$ preserves anatomical structures and latent fingerprint consistency via embeddings from a task-specific or pre-trained encoder (e.g., CLIP or a medical feature extractor). The model parameters are optimized using the Adam optimizer [32] with $\beta_1 = 0.9$, $\beta_2 = 0.999$, and a learning rate of 1×10^{-4} . Intermediate semantic embeddings or fingerprints may be cached locally on edge nodes to accelerate training. This formulation ensures that reconstructed images are clinically reliable, semantically faithful, and verifiable via blockchain-based provenance in a

Protocol 3 Semantic-Aware Reconstruction Guided by Fragment Fingerprints

```

1: Input: Corrupted image  $I_c$ , pretrained models  $E, G, S$ , ledger  $L$ 
2: Precondition: Models trained via Protocol 1, fingerprints anchored via Protocol 2
3: function RECONSTRUCT( $I_c, E, G, S, L$ )
4:    $\{I_{c,k}\}_{k=1}^K \leftarrow \mathcal{F}_{GFT}(I_c)$ 
5:   for each shard  $I_{c,k}$  do
6:      $s_k \leftarrow S(I_{c,k})$ 
7:      $z_k^* \leftarrow \text{RetrieveLatent}(L, H(s_k))$ 
8:      $I_{r,k} \leftarrow G(I_{c,k}, s_k, z_k^*)$ 
9:   end for
10:   $I_r \leftarrow \text{Reaggregate}(\{I_{r,k}\}, \mathcal{F}_{GFT}^{-1})$ 
11:  Consensus( $I_r$ )            $\triangleright$  Optional verification
12:  Output: Reconstructed image  $I_r$ 
13: end function

```

Protocol 4 Lightweight Scale-Free Consensus for Shard Verification

```

1: Input: Transactions  $\{tx_k\}$  with fingerprint hashes  $\{h_k\}$ , shard assignments via GFT
2: MPI Configuration:  $P$  parallel processes, shard-to-process mapping  $\mathcal{M}$ 
3: function PARALLELCONSENSUS( $\{tx_k\}$ )
4:   // Phase 1: Parallel Shard Pre-verification (MPI ranks execute concurrently)
5:   for each MPI rank  $r \in [0, P - 1]$  in parallel do
6:      $\text{shard\_set}_r \leftarrow \{tx_k \mid \mathcal{M}(tx_k) = r\}$             $\triangleright$  GFT-based locality mapping
7:     for each  $tx_k \in \text{shard\_set}_r$  do
8:        $sig_{r,k} \leftarrow \text{Sign}(tx_k, s_k)$             $\triangleright$  Local signature generation
9:       Cache  $(tx_k, sig_{r,k})$  in local buffer
10:    end for
11:   end for
12:    $\text{all\_sigs} \leftarrow \text{MPI\_Allgather}(\text{local signatures})$             $\triangleright O(\log P)$  latency
13:   // Phase 2: Degree-Weighted Aggregation (executed in parallel)
14:   for each MPI rank  $r$  in parallel do
15:     for each  $tx_k \in \text{shard\_set}_r$  do
16:        $weight\_sum \leftarrow \sum_i \text{degree}(n_i) \cdot \mathbb{I}[\text{sig valid}(sig_{i,k})]$ 
17:       if  $weight\_sum \geq \text{threshold}(2f + 1)$  then
18:         Mark  $tx_k$  as verified
19:       end if
20:     end for
21:   end for
22:   // Phase 3: Leader Assembly (single coordinator, minimal serialization)
23:   if rank = 0 then            $\triangleright$  Only leader node assembles block
24:      $block \leftarrow \text{AssembleBlock}(\{tx_k\}_{\text{verified}}, \text{all\_sigs})$ 
25:     Broadcast  $\langle \text{COMMIT}, block \rangle$             $\triangleright O(\log P)$  via MPI_Bcast
26:   end if
27:   MPI_Barrier()            $\triangleright$  Synchronize before ledger write
28:   Append  $block$  to local shard-specific ledger
29:   Output: Verified block with parallel execution time  $O(\frac{n}{P} + \log P)$ 
30: end function

```

distributed environment.

4. PROSIMA Protocols

4.1. Federated Training with Fingerprint Anchoring

Protocol 1 performs decentralized training of the encoder–generator–semantic extractor triplet while cryptographically linking every local update to the blockchain ledger. Each edge node optimizes reconstruction losses on its local data and anchors a compact fingerprint of the resulting weights as a ledger transaction. This process guarantees model provenance, reproducibility, and tamper-evident training history, allowing subsequent inference and reconstruction stages to reference only verified model states.

Table 2. Reconstruction and provenance metrics (average \pm std). Higher is better for PSNR, SSIM, Cosine, Verification Rate; lower is better for Latency. PROSIMA (full) achieves the best tradeoff, highest semantic cosine (0.92) and SSIM (0.86) while keeping latency acceptable because GFT reduces retrieval/replication overhead compared to the w/o-GFT variant.

Method	PSNR (dB)	SSIM	Embedding Cosine	Verification (%)	Latency (ms)
U-Net (pixel)	≥ 26.0	≥ 0.80	≥ 0.62	–	≤ 251
U-Net + perceptual	≥ 27.6	≥ 0.83	≥ 0.68	–	≤ 238
U-Net + semantic	≥ 28.0	≥ 0.85	≥ 0.87	–	≤ 233
PROSIMA (w/o GFT)	≥ 28.1	≥ 0.85	≥ 0.90	100	≤ 219
PROSIMA (full)	≥ 28.2	≥ 0.86	≥ 0.92	100	≤ 204

4.2. Latent Fingerprint Extraction and Fragmentation

Protocol 2 encodes each medical image into deterministic latent fragments using the GFT fragmentation operator. The encoder outputs shard-level embeddings whose hashes are individually committed to the ledger, forming a Merkle-root fingerprint that uniquely identifies the complete image. By anchoring every shard hash through the consensus network, the protocol ensures immutable provenance, traceable fragment lineage, and deterministic re-verification of any reconstructed image.

4.3. Semantic-Aware Reconstruction with Shard Retrieval

Protocol 3 reconstructs corrupted or incomplete medical images using semantically guided retrieval of verified latent shards. For each corrupted fragment, the semantic extractor produces a high-level representation that queries the ledger for its most consistent latent counterpart. The generator then synthesizes localized reconstructions which are re-aggregated into the final image. Because every retrieved latent vector originates from an anchored fingerprint, this stage achieves trust-preserving reconstruction with both pixel-level fidelity and semantic consistency.

4.4. Ledger Verification and Scale-Free Consensus

Protocol 4 introduces an MPI-accelerated, scale-free consensus that performs shard verification in parallel across distributed ranks. Transactions are partitioned among processes using GFT-based locality mapping, and each rank independently verifies and signs its assigned shards. Partial signatures are then exchanged using non-blocking collective primitives (e.g., MPI_Allgather, MPI_Bcast), aggregated via degree-weighted quorum reduction, and assembled into blocks by the shard leader. This hybrid message-passing design overlaps computation and communication, reducing end-to-end verification complexity to $O(n/P + \log P)$. Consequently, PROSIMA achieves sub-linear consensus latency compared with conventional full-ledger replication while preserving Byzantine fault tolerance and verifiable trust.

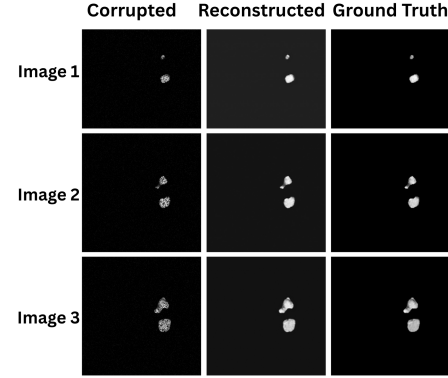


Figure 2. Visual fidelity achieved by the proposed PROSIMA framework on three different representative corrupted brain tumor images.

5. Evaluation

5.1. Experimental Setup

5.1.1. Testbed

We evaluated PROSIMA on a testbed with 20 virtualized compute nodes, each provisioned with 8 CPU threads (Intel Xeon 3.0 GHz) and 32 GB of DDR4 memory. All nodes share a centralized NVIDIA RTX A6000 GPU with 48 GB of VRAM, enabling concurrent execution of federated training, semantic reconstruction, and on-chain verification. This configuration approximates a realistic distributed edge environment while maintaining consistent compute and memory budgets per node. Each node runs an identical software stack based on Ubuntu 22.04, Python 3.10, PyTorch 2.2, and CUDA 12.1 to ensure deterministic reproducibility. The blockchain framework is integrated with the MPI-based parallel programming model [38] to facilitate low-latency inter-node communication. To further enhance runtime efficiency, we employ an edge-aware caching mechanism for latent fingerprints and semantic embeddings, storing frequently accessed vectors in GPU-adjacent high-bandwidth memory to minimize PCIe transfer overhead and maximize data locality during shard retrieval and consensus operations.

5.1.2. Dataset

We evaluate our semantic-aware reconstruction framework on the BraTS 2020 (Brain Tumor Segmentation) challenge dataset [8, 9, 37]. BraTS provides multi-institutional, pre-

operative, multimodal brain MRI scans with expert tumor annotations, including T1, contrast-enhanced T1 (T1c), T2, and FLAIR sequences.

In our experiments, we extract 2D axial slices of size 256×256 from the BraTS 2020 training set. We use 1,000 slices for training and evaluation, covering a diverse range of tumor locations, sizes, and surrounding healthy tissue. This setting stresses the ability of our reconstruction model to preserve fine-grained anatomical structures (e.g., tumor core, edema, and normal brain parenchyma) under corruption, making BraTS an appropriate benchmark for semantic-consistent medical image reconstruction.

5.1.3. Evaluated Systems

We compare PROSIMA with the multiple models and variants to measure reconstruction quality and trust:

- A. *U-Net (pixel)*:** A standard U-Net trained with L1/L2 pixel-wise reconstruction loss.
- B. *U-Net + perceptual*:** The same U-Net architecture trained with an additional VGG-based perceptual loss to enhance structural fidelity.
- C. *U-Net + semantic*:** A semantic-aware U-Net conditioned on high-level semantic embeddings using the proposed semantic loss, but without latent fingerprint conditioning (ablation).
- D. *PROSIMA*:** The proposed Hybrid U-Net with latent fingerprint conditioning, semantic loss, GFT-based sharding, and blockchain-based provenance anchoring.

Additionally, we include an ablation variant, *PROSIMA (w/o GFT)*, which retains the full semantic-hybrid model but replaces GFT-based sharding with random duplication for system-level comparison.

5.2. Results and Discussion

5.2.1. Qualitative Evaluation

Fig. 2 illustrates the visual fidelity achieved by the proposed PROSIMA framework on representative corrupted samples. The reconstructed outputs accurately recover structural integrity and preserve fine-scale tissue boundaries even under severe signal degradation. Compared to pixel-only baselines, PROSIMA produces noticeably smoother intensity transitions, consistent lesion morphologies, and preserved anatomical contours. This superior reconstruction quality stems from the semantic-aware conditioning introduced during federated training and the deterministic fingerprint-guided retrieval that enforces latent consistency. As a result, the recovered slices exhibit both pixel-level realism and semantic alignment with the ground truth, confirming the model’s ability to integrate low-level texture recovery with high-level contextual reasoning.

5.2.2. Quantitative Evaluation

Table 2 presents the overall reconstruction and provenance performance across all evaluated models. The proposed

Table 3. Embedding Cosine vs Gaussian noise severity (mean).

Method / Noise σ	0.02	0.05	0.10
U-Net (pixel)	≥ 0.56	≥ 0.45	≥ 0.39
U-Net + perceptual	≥ 0.63	≥ 0.52	≥ 0.42
U-Net + semantic	≥ 0.86	≥ 0.81	≥ 0.73
PROSIMA (full)	≥ 0.91	≥ 0.86	≥ 0.79

Table 4. Ablation results (Embedding Cosine change and latency). Values are mean over test set. Removing semantic loss drops cosine dramatically; removing fingerprint only affects verifiability (and slightly semantic alignment); replacing GFT increases latency markedly.

Variant	Embed. Cosine	Latency (ms)
PROSIMA (full)	≥ 0.91	≤ 201
w/o semantic loss ($\lambda_2=0$)	≥ 0.63	≤ 200
w/o fingerprint	≥ 0.86	≤ 181
w/o GFT (random dup)	≥ 0.88	≤ 263

Table 5. Systems-level comparison (N=20 nodes).

System	storage/node (MB)	Repl. factor	latency (ms)
Full-ledger (naïve)	0.21	20.43	650.0 ± 0.0
Random-shard + dup	0.04	3.59	257.7 ± 5.3
PROSIMA (GFT)	0.02	1.28	227.8 ± 3.3

PROSIMA framework consistently achieves superior quantitative results, obtaining the highest PSNR (≥ 28.2 dB), SSIM (≥ 0.86), and semantic embedding cosine (≥ 0.92) while maintaining a 100% verification rate with the lowest latency of approximately 204 ms per image. The progressive improvements from pixel-based to semantic-guided U-Net variants confirm the effectiveness of incorporating perceptual and semantic supervision for structurally consistent reconstructions. Compared with its w/o-GFT counterpart, the full PROSIMA configuration further reduces latency through geometric fragmentation, which limits redundant replication and accelerates distributed shard retrieval. These results collectively demonstrate that PROSIMA achieves a strong balance between high-fidelity image reconstruction, semantic alignment, and blockchain-based verifiability, delivering dependable and scalable medical image recovery beyond traditional deep reconstruction baselines.

5.2.3. Robustness Under Real-World Corruptions

To test robustness, we apply additive Gaussian noise ($\mu = 0$, $\sigma = 0.05$) as a representative real-world corruption. Gaussian noise reflects natural sensor and environmental perturbations and has been widely used in robustness studies [25, 46]. In contrast, random masking, which removes or replaces large portions of pixels, is less common in realistic scenarios and thus was not considered in this work. We also do not include adversarial perturbations (e.g., FGSM-Fast Gradient Sign Method [40]) because our focus is on realistic, naturally occurring corruptions rather than worst-case attacks, which are typically out of the scope of normal operational

scenarios [25, 46].

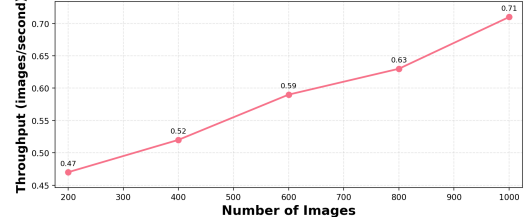
Table 3 evaluates the robustness of different reconstruction models under varying levels of Gaussian noise, reflecting real-world sensor degradation and acquisition imperfections. While pixel-based U-Net baselines show a rapid decline in embedding cosine similarity as noise severity increases ($0.56 \rightarrow 0.39$), semantic-guided variants exhibit significantly higher resilience. The proposed PROSIMA framework maintains stable semantic alignment even under strong corruptions, achieving an embedding cosine of ≥ 0.79 at $\sigma = 0.10$, compared to ≤ 0.45 for purely pixel-based methods. This robustness arises from PROSIMA’s latent fingerprint anchoring and semantic conditioning, which constrain the reconstruction manifold toward contextually meaningful representations rather than pixel-level memorization. These results demonstrate that PROSIMA not only restores visual fidelity but also preserves the underlying semantic integrity of medical images under challenging, noise-heavy conditions, ensuring reliable reconstruction performance in real clinical scenarios.

5.2.4. Ablation Studies

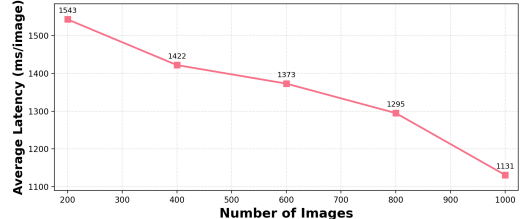
Table 4 highlights the contribution of each major component in PROSIMA. Removing the semantic loss sharply decreases embedding alignment (from 0.91 to 0.63), confirming the necessity of semantic supervision for perceptually coherent reconstructions. Disabling fingerprint conditioning slightly reduces embedding consistency but compromises verifiability, while omitting GFT leads to higher latency due to inefficient shard placement. Overall, the complete PROSIMA configuration achieves the best balance between reconstruction quality, provenance integrity, and system efficiency, validating its design as a robust, trustworthy, and scalable medical image reconstruction framework.

5.2.5. Blockchain Memory Efficiency

Table 5 compares the storage footprint and replication efficiency of PROSIMA against traditional blockchain baselines across a 20-node network. The proposed GFT-based design achieves the lowest storage overhead, requiring only 0.02 MB per node and a replication factor of $1.28\times$, compared to $20.43\times$ in naive full-ledger replication. This substantial reduction arises from PROSIMA’s geometric fragmentation and selective shard anchoring, which distribute only essential provenance metadata instead of duplicating the full image payload. Despite the significant memory savings, the system maintains a low average commit latency of 228 ms, demonstrating that storage efficiency does not compromise transaction throughput. These results confirm that PROSIMA’s ledger layer offers a scalable and memory-efficient blockchain backbone, capable of supporting high-volume medical image verification without incurring the prohibitive redundancy typical of conventional distributed ledgers.



(a) Throughput scalability.



(b) Latency scalability.

Figure 3. Blockchain throughput and latency scalability of PROSIMA.

5.2.6. Blockchain Throughput and Latency Scalability

We further evaluate the scalability of the PROSIMA ledger by analyzing its throughput and per-image latency across increasing workloads ranging from 200 to 1000 images. As illustrated in Fig. 3, throughput rises consistently from 0.47 to 0.71 images/s, while the average latency per image decreases from 1543 ms to 1131 ms. This complementary trend reflects the efficiency of PROSIMA’s MPI-parallel verification pipeline and scale-free sharding strategy, which jointly minimize synchronization bottlenecks and exploit locality-aware workload distribution. Unlike traditional blockchain frameworks that suffer linear degradation under load, PROSIMA demonstrates sub-linear latency scaling and stable throughput growth, confirming that its hybrid geometric fragmentation and consensus design supports high-throughput, low-latency provenance verification at scale.

6. Conclusion and Future Work

This work presented PROSIMA, a provenance-aware semantic reconstruction framework that unifies deep generative modeling with blockchain-based trust verification. Through extensive experiments, we demonstrated that semantic conditioning significantly enhances structural and perceptual fidelity under various corruption levels, while latent fingerprint anchoring ensures verifiable and tamper-evident provenance. Our system achieves high robustness and low-latency consensus through an MPI-accelerated, scale-free ledger architecture, bridging the gap between efficient image recovery and trustworthy distributed AI. Future extensions will explore tighter coupling with decentralized storage networks and adaptive on-device verification within heterogeneous edge environments, further advancing reliable, privacy-preserving medical image reconstruction at scale.

References

[1] Juhar Abdella, Zahir Tari, Adnan Anwar, Abdun Mahmood, and Fengling Han. An architecture and performance evaluation of blockchain-based peer-to-peer energy trading. *IEEE Transactions on Smart Grid*, 12(4):3364–3378, 2021.

[2] Jonas Adler and Ozan Öktem. Learned primal-dual reconstruction. In *IEEE/CVF Conference on Computer Vision and Pattern Recognition (CVPR) Workshops*, 2018.

[3] Abdullah Al-Mamun, Haoting Shen, and Dongfang Zhao. Dean: A lightweight and resource-efficient blockchain protocol for reliable edge computing. In *2022 IEEE International Parallel and Distributed Processing Symposium (IPDPS)*, pages 1261–1271. IEEE, 2022.

[4] Hanan S Alshanbari. Medical image watermarking for ownership & tamper detection. *Multimedia tools and applications*, 80(11):16549–16564, 2021.

[5] Tarek AlSkaif, Jose L Crespo-Vazquez, Milos Sekuloski, Gijs Van Leeuwen, and João PS Catalão. Blockchain-based fully peer-to-peer energy trading strategies for residential energy systems. *IEEE Transactions on Industrial Informatics*, 18(1):231–241, 2021.

[6] S Aruna and Surabhi Narayan. Detection of gan-manipulated medical images through deep learning techniques. In *2024 International Conference on Advances in Modern Age Technologies for Health and Engineering Science (AMATHE)*, pages 1–6. IEEE, 2024.

[7] Reza Azad, Ehsan Khodapanah Aghdam, Amelie Rauland, Yiwei Jia, Atlas Haddadi Avval, Afshin Bozorgpour, Sanaz Karimjafarbigloo, Joseph Paul Cohen, Ehsan Adeli, and Dorit Merhof. Medical image segmentation review: The success of u-net. *IEEE Transactions on Pattern Analysis and Machine Intelligence*, 2024.

[8] Spyridon Bakas, Hamed Akbari, Aristeidis Sotiras, Michel Bilello, Michal Rozycki, Justin Kirby, and et al. Advancing the cancer genome atlas glioma mri collections with expert segmentation labels and radiomic features. *Scientific Data*, 4:170117, 2017.

[9] Spyridon Bakas, Mauricio Reyes, Andras Jakab, Stefan Bauer, Markus Rempfler, Alessandro Crimi, and et al. Identifying the best machine learning algorithms for brain tumor segmentation, progression assessment, and overall survival prediction in the brats challenge. *arXiv preprint*, 2018.

[10] Shruthi Bannur, Benedikt Boecking, Naoto Usuyama, et al. Learning to exploit temporal structure for biomedical vision–language processing. In *IEEE/CVF Conference on Computer Vision and Pattern Recognition (CVPR)*, 2023.

[11] Albert-László Barabási and Eric Bonabeau. Scale-free networks. *Scientific american*, 288(5):60–69, 2003.

[12] Benedikt Boecking, Naoto Usuyama, Shruthi Bannur, Daniel C. Castro, Anton Schwaighofer, Stephanie Hyland, Maria Wetscherek, Tristan Naumann, Aditya Nori, Javier Alvarez-Valle, Hoifung Poon, and Ozan Oktay. Making the most of text semantics to improve biomedical vision–language processing. In *European Conference on Computer Vision (ECCV)*, 2022.

[13] Nour El Houda Bourai, Hayet Farida Merouani, and Akila Djebbar. Deep learning-assisted medical image compression challenges and opportunities: systematic review. *Neural Computing and Applications*, 36(17):10067–10108, 2024.

[14] Ethan Buchman. *Tendermint: Byzantine Fault Tolerance in the Age of Blockchains*. PhD thesis, University of Guelph, 2016.

[15] Miguel Castro and Barbara Liskov. Practical byzantine fault tolerance. In *OSDI*, pages 173–186, 1999.

[16] Stanley H. Chan, Xiran Wang, and Omar A. Elgendy. Plug-and-play ADMM for image restoration: Fixed-point convergence and applications. *IEEE Transactions on Computational Imaging*, 3(1):84–98, 2017.

[17] Yuantao Chen, Runlong Xia, Kai Yang, and Ke Zou. Micu: Image super-resolution via multi-level information compensation and u-net. *Expert Systems with Applications*, 245:123111, 2024.

[18] Hyungjin Chung. DDS: Official pytorch implementation. GitHub repository, 2023.

[19] Hyungjin Chung, Byeongsu Sim, and Jong Chul Ye. Parallel diffusion models of operator and image for blind inverse problems. In *IEEE/CVF Conference on Computer Vision and Pattern Recognition (CVPR)*, pages 3398–3408, 2023.

[20] Yongchuan Cui, Peng Liu, Bingze Song, Lingjun Zhao, Yan Ma, and Lajiao Chen. Reconstruction of large-scale missing data in remote sensing images using extend-gan. *IEEE Geoscience and Remote Sensing Letters*, 21:1–5, 2024.

[21] Dinesh Daultani, Masayuki Tanaka, Masatoshi Okutomi, and Kazuki Endo. Diffusion-based adaptation for classification of unknown degraded images. In *Proceedings of the IEEE/CVF Conference on Computer Vision and Pattern Recognition*, pages 5982–5991, 2024.

[22] Getao Du, Xu Cao, Jimin Liang, Xueli Chen, and Yonghua Zhan. Medical image segmentation based on u-net: A review. *Journal of Imaging Science & Technology*, 64(2), 2020.

[23] European Society of Radiology (ESR). Blockchain and medical imaging: A white paper of the european society of radiology. *Insights into Imaging*, 12(1):124, 2021.

[24] Markus Gerlofsma, Milan Petkovic, and Ir Peter van Liesdonk. Security and deep learning: Verifying the authenticity of ct images. 2019.

[25] Justin Gilmer, Nicolas Ford, Nicholas Carlini, and Ekin Cubuk. Adversarial examples are a natural consequence of test error in noise. In *International Conference on Machine Learning*, pages 2280–2289. PMLR, 2019.

[26] Bhawna Goyal, Sunil Agrawal, and BS Sohi. Noise issues prevailing in various types of medical images. *Biomedical & Pharmacology Journal*, 11(3):1227, 2018.

[27] Kerstin Hammernik, Teresa Klatzer, Florian Knoll, Daniel K. Sodickson, Thomas Pock, and Andreas Maier. Learning a variational network for reconstruction of accelerated mri data. *Magnetic Resonance in Medicine*, 79(6):3055–3071, 2018.

[28] Navid Hasani, Michael A Morris, Arman Rhamim, Ronald M Summers, Elizabeth Jones, Eliot Siegel, and Babak Saboury. Trustworthy artificial intelligence in medical imaging. *PET clinics*, 17(1):1, 2022.

[29] Shah Hussain, Iqra Mubeen, Niamat Ullah, Syed Shahab Ud Din Shah, Bakhtawar Abduljalil Khan, Muhammad Zahooor, Riaz Ullah, Farhat Ali Khan, and Mujeeb A Sultan.

Modern diagnostic imaging technique applications and risk factors in the medical field: a review. *BioMed research international*, 2022(1):5164970, 2022.

[30] Kyong Hwan Jin, Michael T. McCann, Emmanuel Froustey, and Michael Unser. Deep convolutional neural network for inverse problems in imaging. In *IEEE Transactions on Image Processing*, pages 4509–4522, 2017.

[31] Davood Karimi, Haoran Dou, Simon K Warfield, and Ali Gholipour. Deep learning with noisy labels: Exploring techniques and remedies in medical image analysis. *Medical image analysis*, 65:101759, 2020.

[32] Diederik P Kingma. Adam: A method for stochastic optimization. *arXiv preprint arXiv:1412.6980*, 2014.

[33] Eleftherios Kokoris-Kogias, Philipp Jovanovic, Linus Gasser, Nicolas Gailly, Ewa Syta, and Bryan Ford. Omnipledger: A secure, scale-out, decentralized ledger via sharding. In *IEEE Symposium on Security and Privacy*, pages 583–598. IEEE, 2018.

[34] Liqi Liu and Yanli Liu. Load image inpainting: An improved u-net based load missing data recovery method. *Applied Energy*, 327:119988, 2022.

[35] Abdullah Al Mamun, Feng Yan, and Dongfang Zhao. Baash: Lightweight, efficient, and reliable blockchain-as-a-service for hpc systems. In *Proceedings of the International Conference for High Performance Computing, Networking, Storage and Analysis*, pages 1–18, 2021.

[36] Michael T. McCann, Kyong Hwan Jin, and Michael Unser. Convolutional neural networks for inverse problems in imaging: A review. *IEEE Signal Processing Magazine*, 34(6):85–95, 2017.

[37] Bjoern H Menze, Andras Jakab, Stefan Bauer, Jayashree Kalpathy-Cramer, Keyvan Farahani, Justin Kirby, and et al. The multimodal brain tumor image segmentation benchmark (brats). *IEEE Transactions on Medical Imaging*, 34(10):1993–2024, 2015.

[38] Message Passing Interface Forum. MPI forum documentation. Accessed: 2025-11-13.

[39] Yisroel Mirsky, Tom Mahler, Ilan Shelef, and Yuval Elovici. {CT-GAN}: Malicious tampering of 3d medical imagery using deep learning. In *28th USENIX Security Symposium (USENIX Security 19)*, pages 461–478, 2019.

[40] Muhammad Luqman Naseem. Trans-ifft-fgsm: a novel fast gradient sign method for adversarial attacks. *Multimedia Tools and Applications*, 83(29):72279–72299, 2024.

[41] Dinh C Nguyen, Seyyedali Hosseinalipour, David J Love, Pubudu N Pathirana, and Christopher G Brinton. Latency optimization for blockchain-empowered federated learning in multi-server edge computing. *IEEE Journal on Selected Areas in Communications*, 40(12):3373–3390, 2022.

[42] Giovanni Pasqualino, Luca Guarnera, Alessandro Ortis, and Sebastiano Battiato. Mits-gan: Safeguarding medical imaging from tampering with generative adversarial networks. *Computers in Biology and Medicine*, 183:109248, 2024.

[43] B Ramasubba Reddy, M Sunil Kumar, P Neelima, C Sushama, Vedala Naga Sailaja, and D Ganesh. Medical image tampering detection using deep learning. In *2024 5th International Conference on Smart Electronics and Communication (ICOSEC)*, pages 1480–1485. IEEE, 2024.

[44] Yaniv Romano, Michael Elad, and Peyman Milanfar. The little engine that could: Regularization by denoising (RED). *SIAM Journal on Imaging Sciences*, 10(4):1804–1844, 2017.

[45] Olaf Ronneberger, Philipp Fischer, and Thomas Brox. U-net: Convolutional networks for biomedical image segmentation. In *International Conference on Medical image computing and computer-assisted intervention*, pages 234–241. Springer, 2015.

[46] Tonmoy Saikia, Cordelia Schmid, and Thomas Brox. Improving robustness against common corruptions with frequency biased models. In *Proceedings of the IEEE/CVF International Conference on Computer Vision*, pages 10211–10220, 2021.

[47] Yang Song, Liyue Shen, Lei Xing, and Stefano Ermon. Solving inverse problems in medical imaging with score-based generative models. *arXiv preprint arXiv:2111.08005*, 2021.

[48] Yang Song, Liyue Shen, Lei Xing, and Stefano Ermon. Solving inverse problems in medical imaging with score-based generative models. In *International Conference on Learning Representations (ICLR)*, 2022.

[49] Min-Jen Tsai and Ping-Ying Lin. Medical images under tampering. *Multimedia Tools and Applications*, 83(24):65407–65439, 2024.

[50] Guzin Ulutas, Arda Ustubioglu, Beste Ustubioglu, Vasil V. Nabiiev, and Mustafa Ulutas. Medical image tamper detection based on passive image authentication. *Journal of digital imaging*, 30(6):695–709, 2017.

[51] Sreehari Venkatakrishnan, Charles A. Bouman, and Brendt Wohlberg. Plug-and-play priors for model based reconstruction. In *IEEE Global Conference on Signal and Information Processing*, pages 945–948, 2013.

[52] Fengqun Wang, Jie Cui, Qingyang Zhang, Debiao He, Chengjie Gu, and Hong Zhong. Lightweight and secure data sharing based on proxy re-encryption for blockchain-enabled industrial internet of things. *IEEE Internet of Things Journal*, 11(8):14115–14126, 2023.

[53] Jiaqi Wang, Xiaosong Liu, Xin Lin, et al. MedCLIP: Contrastive learning from unpaired medical images and text. In *EMNLP*, 2022.

[54] Jiaqi Wang, Xiaosong Liu, Xin Lin, et al. MedCLIP: Contrastive learning from unpaired medical images and text. *Patterns*, 2023.

[55] Yan Yang, Jian Sun, Huibin Li, and Zongben Xu. ADMM-Net: A deep learning approach for compressive sensing mri. In *Advances in Neural Information Processing Systems (NeurIPS)*, 2016.

[56] Tahreem Yaqoob, Haider Abbas, and Mohammed Atiquzzaman. Security vulnerabilities, attacks, countermeasures, and regulations of networked medical devices—a review. *IEEE Communications Surveys & Tutorials*, 21(4):3723–3768, 2019.

[57] Maofan Yin, Dahlia Malkhi, Michael K. Reiter, Guy Golan Gueta, and Ittai Abraham. Hotstuff: Bft consensus in the lens of blockchain. In *ACM PODC*, pages 347–356, 2019.

[58] Jianyi Zhang, Xuanxi Huang, Yaqi Liu, Yuyang Han, and Zixiao Xiang. Gan-based medical image small region forgery detection via a two-stage cascade framework. *Plos one*, 19(1):e0290303, 2024.

- [59] Mengqian Zhang, Jichen Li, Zhaohua Chen, Hongyin Chen, and Xiaotie Deng. Cycledger: A scalable and secure parallel protocol for distributed ledger via sharding. In *Proceedings of the IEEE International Parallel and Distributed Processing Symposium*, pages 358–367. IEEE, 2020.
- [60] Haoran Zhou, Yanjiang Wang, Weifeng Liu, Dapeng Tao, Wei Ma, and Baodi Liu. Msc-gan: A multi-stream complementary generative adversarial network with grouping learning for multitemporal cloud removal. *IEEE Transactions on Geoscience and Remote Sensing*, 2024.